Absolute and total electron-capture cross sections in slow Ar^{q+}-C_{60} collisions

S. H. Schwartz, A. Fardi, K. Haghighat, A. Langereis, H. T. Schmidt, and H. Cederquist
Stockholm University, Frescativägen 24, S-104 05 Stockholm, Sweden
(Received 27 April 2000; published 8 December 2000)

We present experimental absolute and total electron-capture cross sections for Ar^{q+}-C_{60} ($q=4$, 6, and 8–18) collisions at $3.3q$ keV. The absolute scale is based on the C_{60} vapor pressure by Abrefah *et al.* [Appl. Phys. Lett. **60**, 1313 (1992)], which together with the results of Mathews *et al.* [J. Phys. Chem. **96**, 3566, (1992)] are the only possible choices among the many, widely dispersed, vapor pressures reported in the literature. In order to support this statement, we calculate total electron-capture cross sections modeling C_{60} as a pointlike object and as an infinitely conducting sphere (ICS). These model results are shown to differ little, since polarization and finite-size effects are relatively unimportant for the distant collisions at which the outermost (first) electrons are transferred. We are thus able to use the semiempirical formula for absolute ion-*atom* cross sections by Selberg *et al.* [Phys. Rev. A **54**, 4127 (1996)], treating C_{60} as a hypothetical atom with ionization potential $I_1=7.6$ eV, and the ICS model to define lower and upper bounds for the absolute cross-section scale. We find significant oscillations in the total electron-capture cross sections as functions of q.

DOI: 10.1103/PhysRevA.63.013201 PACS number(s): 36.40.−c, 34.70.+e, 34.50.Fa

I. INTRODUCTION

So far only three experiments reported on absolute electron capture cross sections for *slow highly charged ions* colliding with C_{60}. Walch *et al.* [1] determined absolute cross sections σ_q^s for capture of s electrons to 80-keV Ar^{8+} projectiles, yielding a total electron-capture cross section of $(4.4\pm1.8)\times10^{-14}$ cm^2. Their absolute scale was set by means of the C_{60} vapor pressure by Abrefah *et al.* [2]. Using the same result [2], Selberg *et al.* [3] determined the cross sections $4.6\pm1.4(q=8)$, $10.1\pm2.8(q=13)$, $7.1\pm2.0(q=14)$, and $(10.0\pm3.1)\times10^{-14}$ cm^2 ($q=15$) for $3.3q$-keV Ar^{q+}-C_{60} collisions. The Ar^{8+} results by Walch *et al.* [1] and Selberg *et al.* [3] agree as expected [4] in this velocity regime. In addition, Larsson *et al.* [5] reported absolute cross sections, based on Ref. [2], for single- and multiple-electron capture in 100-keV Ar^{q+}, Xe^{q+}, and He^{q+}-C_{60} collisions with $q\leqslant4$.

Absolute experimental cross sections were also quoted by, e.g., Baba *et al.* [6,7], Vostrikov *et al.* [8], Tarnovsky *et al.* [9], and Matt *et al.* [10] for electron-impact ionization of C_{60} and by, e.g., Gong *et al.* [11], Smith [12], and Coheur *et al.* [13] for photoabsorption in C_{60}. In the latter studies [11–13], the authors used the vapor pressure by Piacente *et al.* [14] to set their absolute scales. Baba *et al.* [6,7] and Vostrikov *et al.* [8] relied on the vapor pressure by Mathews *et al.* [15], while the number density was deduced directly from the measured flux of C_{60} molecules in neutral beams in Refs. [9] and [10]. The C_{60} vapor pressure was also reported by, e.g., Popovic *et al.* [16], and very recently by Jaensch *et al.* [17]. A main difficulty in the present work, and in all other studies in which absolute reaction rates and cross sections involving C_{60} targets are determined, is the large spread in literature values for the C_{60} vapor pressure. For our temperature range, $T=420$–$425\,^\circ$C, the results scatter over an order of magnitude from, e.g., 2×10^{-5} Torr [15] to 27×10^{-5} Torr [16] at $T=420\,^\circ$C.

In this work, we will show that it is possible to use simple theoretical arguments and well-established experimental results on absolute and total electron-capture cross sections for ion-*atom* collisions to discriminate between the different vapor pressures of C_{60}. In this way we show that the absolute values of Abrefah *et al.* [2] and Mathews *et al.* [15] at $T=420\,^\circ$C are the only possible choices. Since the former authors report a heat of sublimation, ΔH, in agreement with that measured by Larsson *et al.* [5], using the same preheating procedure (of the C_{60} powder) and type of collision cell as we do, we base our results on Ref. [2].

Here, we have measured charge-exchange yields for

$$Ar^{q+}+C_{60}\rightarrow Ar^{(q-s)+}+C_{60}^{r+}+(r-s)e^- \tag{1}$$

collisions at $3.3q$ keV, where r electrons are removed from C_{60}, and s electrons are stabilized on the projectile. We discriminate between the different values of s and present absolute and total electron capture cross sections

$$\sigma_q^{\rm tot}=\sum_{s=1}^{q}\sigma_q^s \tag{2}$$

for projectile charge states ranging from $q=4$ to $q=18$.

In Sec. II, we present the experimental set-up and method in some detail and estimate the different contributions to the uncertainties in $\sigma_q^{\rm tot}$. Three different models for the electronic response of the C_{60} molecule are briefly described in Sec. III. First, we argue that the movable hole model [18] gives a crude description of the interaction between slow highly charged ions and C_{60} at large distances. Instead, we use the Infinitely conducting sphere (ICS) model (see, e.g., Cederquist *et al.* [18], and references therein) to derive the first critical distance, the binding energy of the projectile capture states, and the corresponding effective principal quantum number. The same quantities are then derived for a much simpler model in which the C_{60} molecule is viewed as an hypothetical atomic target with an ionization potential equal to that of C_{60}. It is shown that the predictions for the total electron-capture cross sections differ little for the two

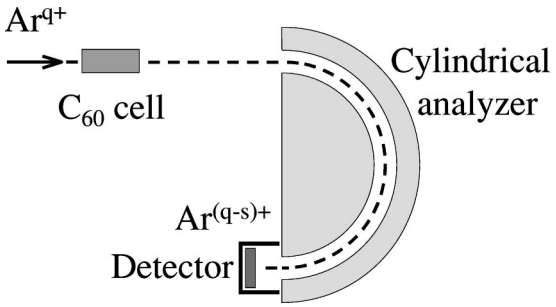

FIG. 1. A schematic of the experimental setup used to measure total electron-capture cross sections σ_q^{tot} in Ar^{q+}-C_{60} collisions. The number of stabilized electrons on the projectile is denoted *s*.

latter models. We thus use the semiempirical formula for ion-*atom* collisions by Selberg *et al.* [19], which gives results slightly below those of the over-the-barrier model for atomic targets [20], to set lower bounds for the true absolute cross sections for Ar^{q+}-C_{60} collisions. The over-the-barrier model combined with the ICS model and a quasicontinuum of projectile capture states are used to define the corresponding upper bounds. We thus arrive at a rather narrow range for the vapor pressure of C_{60} at 420 °C, and through comparisons with Larsson *et al.* [5] we decide to use Ref. [2]. In Sec. V we compare the present absolute and total electron-capture cross sections with earlier results [3]. We report on oscillations in the present cross sections as functions of *q*, which most likely are related to the finite densities of projectile capture states. Finally, we discuss some of the general difficulties associated with C_{60} vapor pressure measurements, and explain how slow highly charged ions may be particularly useful in such measurements.

II. EXPERIMENTAL TECHNIQUES AND PROCEDURES

The argon ions were produced in charge states $q=4$, 6, and 8–18 by the cryogenic electron beam ion source CRYSIS at the Manne Siegbahn Laboratory in Stockholm. The ion beams were transported to the experimental setup by means of electrostatic ion-optical elements and a 90° double-focusing bending magnet. A specific projectile charge state was selected using the magnet and its entrance and exit slits. The beam was then collimated before it entered the experimental setup, which is depicted in Fig. 1.

The selected Ar^{q+} beam enters a 50-mm-long resistively heated stainless-steel cylinder shown in Fig. 2. After the collision cell (the 30-mm central part of the steel cylinder) the ions enter a cylindrical analyzer and are directed toward a multichannel plate detector. The total acceptance angle of the system is ±0.5°, i.e., larger than the widths of the actually measured angular distributions [18,21].

The cell contained 99.9% pure C_{60} powder (Hoechst gold grade), and the temperature was set to $T=420$ or 425 °C, depending on the projectile charge state. The set temperature was stabilized within ±1 °C by means of a thermocouple controlling the power to the heating wire. After charging the cell with C_{60} it was preheated for many hours at $T_{preh}=500$ °C in order to dispose of the solvents. This was also above the critical temperature $T_C=477$ °C, at which a possible phase transition in the C_{60} powder has been reported [13]. We corrected for collisions in the residual gas by measuring the charge exchange at 300 and 350 °C, where the C_{60} target density was shown to be insignificant in, e.g., optical density measurements by Gong *et al.* [11].

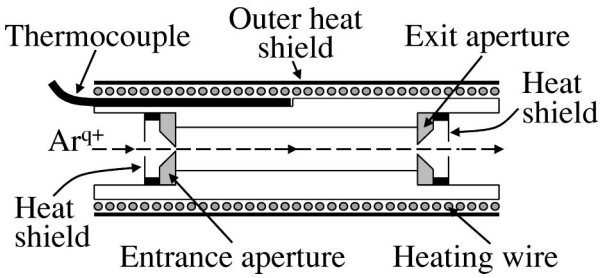

FIG. 2. A central cut through the stainless steel cylinder containing the C_{60} cell, enclosed by 2-mm-thick Cu disks (shaded) with countersink entrance and exit apertures of diameters 0.5 and 1.0 mm, respectively. Thin heat shields are mounted 2 mm outside the apertures. The heating wire is indicated by the gray circles. The thermocouple gauge is embedded in the body of the cylinder. The cylinder and the heating wire are wrapped in an outer heat shield.

The intensity $I(q)$ of a beam of ions remaining in the incoming charge state *q* after passage through the cell with a C_{60} target of density $\rho(T)$ and length *L* is

$$I(q)=I_0(q)\exp(-\rho L\sigma_q^{\mathrm{tot}}). \tag{3}$$

Here $I_0(q)$ is the intensity of the incoming beam before the cell. We thus have

$$\sigma_q^{\mathrm{tot}}=-\frac{k_BT}{p(T)L}\ln\left(\frac{I(q)}{I_0(q)}\right), \tag{4}$$

where k_B is the Boltzmann constant. $I_0(q)$ can be written as a sum of the intensities $I(q-s)$ after the cell:

$$I_0(q)=\sum_{s=0}^{q} I(q-s)=I(q)+\sum_{s=1}^{q} I(q-s). \tag{5}$$

By combining Eqs. (4) and (5) in

$$\sigma_q^{\mathrm{tot}}=\frac{k_BT}{p(T)L}\ln\left(1+\frac{\sum_{s=1}^{q} I(q-s)}{I(q)}\right)$$
$$=\frac{k_BT}{p(T)L}\ln\left(1+\frac{I(q-1)}{I(q)}+\cdots+\frac{I(0)}{I(q)}\right), \tag{6}$$

we may determine σ_q^{tot} by measuring the ratios $I(q-s)/I(q)$ for $s=1$ to $s=q$, or more often to $s=q-1$, at a given preset temperature *T*. The $s=q$ channel, i.e., neutralization of the projectile, was only measured for the Ar^{8+}-case, using a setup with straight deflector plates after the cell [18]. It was then found that this channel contributed less than 1% to the total electron-capture cross section. From the measurements of the cross sections σ_q^s as functions of *s* [22], we conclude that the relative contributions are even

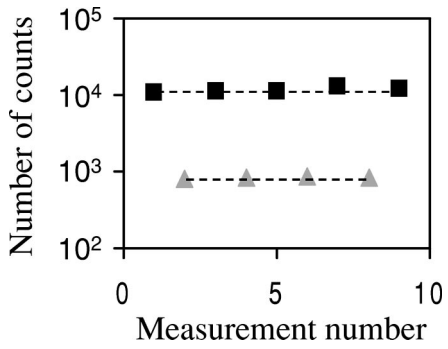

FIG. 3. The measured number of counts due to ions remaining in the incoming charge state ($s=0$; black squares) and ions in the charge-reduced beam ($s=1$; gray triangles) as functions of the measurement number. This example shows results for Ar^{8+}-C_{60} collisions, where each data point was obtained after 100 of acquisition time.

smaller for $q>8$. For $q=4$ and 6, however, the measured total cross sections σ_q^{tot} may be somewhat to low due to the missing neutral components.

The intensities $I(q)$ and $I(q-s)$ are measured alternately several times during short-time intervals, and thus normalization to $I_0(q)$ was not necessary. We have only included results for $I(q-s)/I(q)$ in which the variations in $I(q)$ and $I(q-s)$ were insignificant. An example of a series of measurements with nearly constant incoming beam intensity is shown in Fig. 3.

Multiple-collision corrections are not necessary when considering *total* electron-capture cross sections in slow collisions where electron *loss* from the projectile is negligible. This may be understood by noting that the total charge-exchange yields

$$S_q=\sum_{s=1}^{q} I(q-s)/I(q) \tag{7}$$

in Eq. (6) remain constant whether or not such corrections are made. Multiple collisions will always lower the projectile charge, and will thus shift the measured $I(q-s)$ distribution towards larger s in relation to the true single-collision $I(q-s)$-distribution The sum $\Sigma_{s=1}^{q} I(q-s)$ and $I(q)$ will, however, be unchanged since they are proportional to the probabilities for *at least one* collision and *no* (electron capture) collision, respectively.

The uncertainty in σ_q^{tot} has four contributions. Errors in (i) the absolute temperature T, (ii) the effective length L, and (iii) the sum S_q. Finally, there is in principle a large uncertainty stemming from (iv) the spread in literature values for $p(T)$. In Sec. IV we will show in detail that it indeed is possible to deal with the latter problem and to set the absolute C_{60} vapor pressure scale, while we will consider (i)–(iii) here. Using the Clausius-Clapeyron relation $p(T)=C\exp(-\Delta H/k_BT)$ (see, e.g., Ref. [2]), the relative uncertainty in σ_q^{tot} becomes

$$\frac{\delta\sigma_q^{\mathrm{tot}}}{\sigma_q^{\mathrm{tot}}}=\left[\left(\frac{\delta L}{L}\right)^2+\left(1-\frac{\Delta H}{k_BT}\right)^2\left(\frac{\delta T}{T}\right)^2+\left(\frac{S_q}{(1+S_q)\ln(1+S_q)}\right)^2\left(\frac{\delta S_q}{S_q}\right)^2\right]^{1/2}, \tag{8}$$

where ΔH is the heat of sublimation per C_{60} molecule. We estimate $\delta L/L$ to be $\sim 3\%$. The value of $(1-[\Delta H/k_BT])\delta T/T$ becomes $\sim 2\%$ for $\delta T=1\,^{\circ}\mathrm{C}$ when we use the value of ΔH by Abrefah *et al.* [2] or Larsson *et al.* [5], which are in agreement. The factor in front of $\delta S_q/S_q$ in Eq. (8) is close to 1, and the statistical contributions are around 1% for $q=4$, 6, and 8–17 while it is much higher (about 6%) for $q=18$. The combined uncertainties in $\delta\sigma_q^{\mathrm{tot}}/\sigma_q^{\mathrm{tot}}$ are thus 8% for $q=18\%$ and 6% for all other projectile charge states.

III. MODELS

The movable hole (MH) model for the electronic response of C_{60} was developed independently by several authors [23–25]. In the version used by Cederquist *et al.* [18], it was assumed that the positive charges left behind on the target after electron transfer moved on the molecular surface in a localized fashion towards minimum potential-energy configurations [18]. Projectile energy and angular distributions due to *multiple*-electron transfer were found to agree with the corresponding experimental *and* ICS quantities when the hole-rearrangement times were set to 10^{-16} s or below [18]. The merit of the movable hole model is that it can be used to extract information about time scales for the electronic motion. However, it gives a crude description of the interaction before the transfer of the first electron. There is, e.g., no account of target polarization at large distances [18] and, more seriously, the potential from which the first electron is removed is assumed to be localized to the surface of the molecule. The latter is not consistent with the strongly delocalized character of the outer molecular orbital in C_{60} [26]. Therefore, the MH model does not give realistic *total* electron-capture cross sections and we will not deal with it further in this work. Instead we use the infinitely conducting sphere model to derive the first critical over-the-barrier capture distances and show that it is a fair approximation to treat the C_{60} molecule as a point-like object in calculations of total electron-capture cross sections.

A. Infinitely conducting sphere model

The infinitely conducting sphere model was first used in order to rationalize ion-C_{60} scattering by Walch *et al.* [1] and later by Bárány and Setterlind [20], Thumm [27], Thumm *et al.* [28], and Cederquist *et al.* [18]. A more complete description of the present version of this model can be found in Ref. [18]. Further, the ICS model and closely related dielectric (metal) sphere models have proven to be successful for descriptions of a variety of phenomena including the C_{60} molecules interaction with photons [29] and electrons [30], as well as the rate of radiative cooling of hot negative C_{60} ions [31].

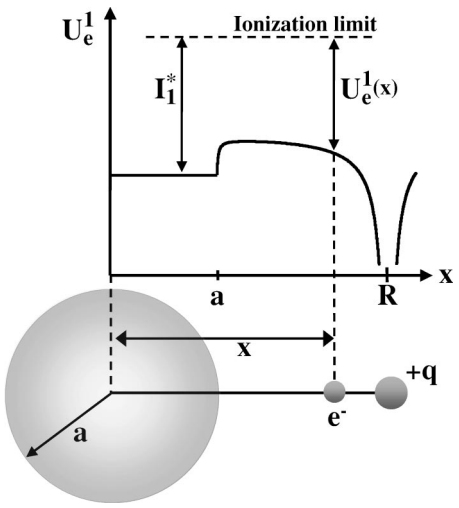

FIG. 4. Definitions of x, R, and a, and a schematic of the potential $U_e^1(x)$. The binding energy of the electron at the target is I_1^* when the projectile is at the distance R (cf. text).

Here we define the radius of the sphere, a, through the experimental polarizability of free C_{60} molecules. The latter quantity was recently measured directly by Antoine *et al.* [32] to be $\alpha_{pol}=76.5\pm 8.0$ Å^3. This result is consistent with $a=8.2a_0$ used by Cederquist *et al.* [18], and we have chosen to use the same value for a also in this work (although the result of Ref. [32] indicate a slightly lower value). The potential energy U_e^1 for an electron between the projectile and the sphere is [18]

$$U_e^1=-\frac{q}{R-x}+\frac{aq}{Rx-a^2}-\frac{aq+R}{Rx}+\frac{1}{2}\left(\frac{a}{x^2}-\frac{a}{x^2-a^2}\right), \tag{9}$$

where x and R are defined in Fig. 4. The first term in Eq. (9) is due to the interaction between the electron and the projectile. The two following terms describe the electrons interaction with the image charges of the projectile and the net charge of the sphere, while the last two terms are the electrons interaction with its self-induced image charges. Potential (9) is identical to the one from the projectile and the real induced inhomogenous surface-charge distribution.

The most important parameter in the present context, i.e., the first critical radius, R_1, is obtained by finding the distance at which the Stark-shifted first ionization potential of the target

$$I_1^*=I_1+q/R \tag{10}$$

equals the maximum of the potential barrier in Eq. (9). In a similar fashion, it is possible to derive critical over-the-barrier distances for the sequential removals of, e.g., a second efection and a third electron from C_{60} [18]. Further, the quasicontinuum approximation may be used here since single-electron transfer populates highly excited states in the projectile, and thus the absorbing sphere picture is valid. All projectile trajectories with distances of closest approach smaller than R_1 will thus lead to the removal of at least one

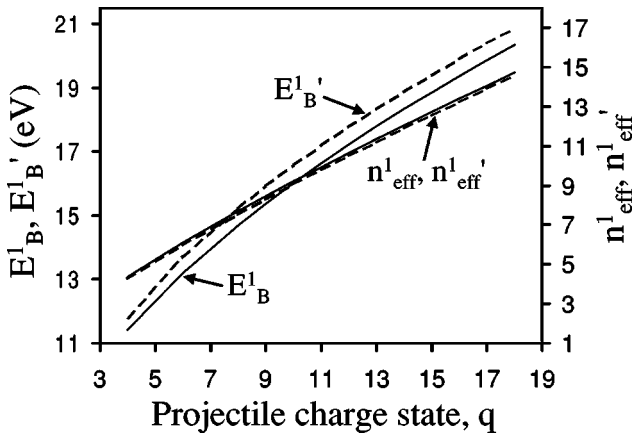

FIG. 5. Left-hand scale: The binding energies E_B^1 and $E_B^{1\prime}$ for the first active electron according to the infinitely conducting sphere and the pointlike target models, respectively. Right-hand scale: The effective principal quantum numbers n_{eff}^1 and $n_{eff}^{1\prime}$ for the same two models. The ICS results are shown as solid curves, and the pointlike target results as dashed curves.

electron from C_{60} and, since we are dealing with low-velocity collisions, at least one of these electrons will be captured by the projectile. The validity of the quasicontinuum approximation is a key point here, and we will thus derive an expression for the effective principal quantum number for single-electron-capture.

Using the quasicontinuum assumption there is a resonant Stark-shifted projectile state available for electron transfer from the outermost Stark shifted target state at $R=R_1$, yielding

$$I_1+\frac{q}{R_1}=E_B^1+\frac{1}{R_1}-\frac{aq}{R_1^2-a^2}+\frac{aq}{R_1^2}-\frac{a}{2R_1^2}+\frac{a}{2(R_1^2-a^2)}. \tag{11}$$

The left-hand side is given by Eq. (10) at $R=R_1$. At infinite values of R the right-hand side becomes E_B^1, which is the binding energy of the electron to the free projectile before relaxation.

From Eq. (11) we obtain

$$E_B^1=\frac{q-1}{R_1}+\frac{a(q-1/2)}{R_1^2-a^2}-\frac{a(q-1/2)}{R_1^2}+I_1, \tag{12}$$

and the effective principal quantum number for single-electron capture becomes $n_{eff}^1=q/\sqrt{2E_B^1}$. In Fig. 5, we show the results for E_B^1 and n_{eff}^1, and confirm that high-n states are populated. We thus arrive at an absorbing sphere cross section for electron capture (including both single- and multiple-electron-capture) of $\sigma_q^{\rm tot}=\pi R_1^2$. The first critical distances R_1 and $\sigma_q^{\rm tot}=\pi R_1^2$ are shown as functions of q in Figs. 6 and 7, respectively. Note that the model cross sections only depend on the (simple) descriptions of single-electron transfer at large distances (via R_1) although they have important contributions also from more complex interactions at closer distances.

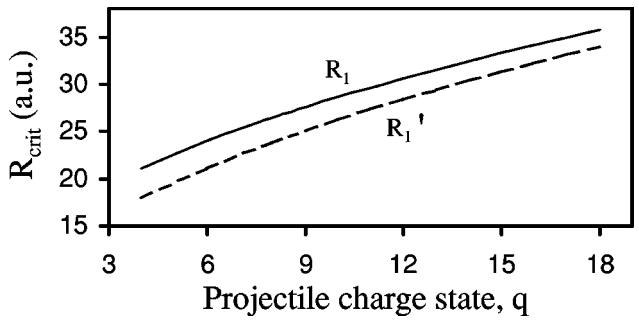

FIG. 6. The critical over-the-barrier distances for transfer of the first electron from C_{60} as functions of q. The solid curve shows the numerical results (R_1), with C_{60} modeled as an infinitely conducting sphere . The dashed curve shows the results (R_1') when treating the C_{60} molecule as a point target with the ionization potential $I_1 = 7.6$ eV.

B. A pointlike target

For large values of q, the critical distances become large, and Eq. (9) reduces to

$$U_e^1 \approx -\frac{q}{R-x} - \frac{1}{x}. \tag{13}$$

The maximum of this approximate potential becomes equal to the Stark-shifted target binding energy [Eq. (10)] at

$$R_1' = (2\sqrt{q}+1)/I_1, \tag{14}$$

which is identical to the expression for an atomic target [33]. Using the quasicontinuum approximation again, we find the resonance condition to be fulfilled as soon as the barrier height becomes low enough to allow the electron to leave the target potential:

$$I_1 + \frac{q}{R_1'} = E_B^{1\prime} + \frac{1}{R_1'}. \tag{15}$$

This expression is identical to Eq. (11), with $a=0$ giving

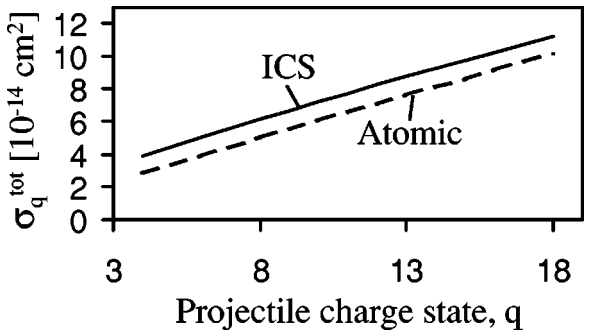

FIG. 7. Absolute and total electron-capture cross sections according to the over-the-barrier model combined with two different models for the electronic response of C_{60}; the infinitely conducting sphere (ICS) model and the pointlike particle model (''Atomic'').

$$E_B^{1\prime} = \frac{q-1}{R_1'} + I_1, \tag{16}$$

and the effective principal quantum numbers for single-electron capture, $n_{eff}^{1\prime} = q/\sqrt{2E_B^{1\prime}}$, are shown in Fig. 5. The first critical distances R_1' and the corresponding absorbing sphere cross sections $\sigma_q^{\rm tot} = \pi R_1'^2$ are shown in Figs. 6 and 7, respectively.

C. Model comparisons

The binding energies E_B^1 and $E_B^{1\prime}$ for the ICS and pointlike target models are compared in Fig. 5, and exhibit small differences of less than 0.5 eV. The effective principal quantum numbers n_{eff}^1 and $n_{eff}^{1\prime}$ are rather high and close, and they range from about 5 for $q=5$ to more than 14 for $q=18$. In the case of single-electron-capture in Ar^{q+}-C_{60} collisions ($q=8$ and 13–15), the over-the-barrier predictions for highly excited capture states were verified experimentally by Selberg *et al.* [3]. The high effective quantum numbers, resulting from both models, strongly indicate that it indeed is reasonable to assume quasicontinua of electron-capture states and, thus, that R_1 and R_1' may be used to calculate geometrical cross sections for electron capture.

In Fig. 6 we compare the first critical distances R_1' and R_1 according to the two models. The latter, R_1, are obtained numerically by finding the internuclear distances at which the maxima of the potential barriers, obtained from Eq. (9), equal the Stark-shifted first ionization potential of the target [Eq. (10)]. In the high-q limit, the relation between R_1 and R_1', with R_1' given by Eq. (14), is approximately

$$R_1 = \left(\frac{q-1}{q-1/2}\right)^{1/4} \frac{R_1'}{1-\left(\frac{a}{R_1'}\right)^2}. \tag{17}$$

In Fig. 7 we show that the differences between $\sigma_q^{\rm tot} = \pi R_1^2$ and $\sigma_q^{\rm tot} = \pi R_1'^2$ are small. We thus conclude that the inclusion of target polarization and finite target size, which are only taken into account in the ICS model, has a minor effect on the model cross section. This result will be used in Sec. IV to motivate our use of the semi-empirical formula for ion-*atom* collisions to set a *lower limit* for the total electron-capture cross section for the C_{60} target.

IV. RESULTS

In 1996 Selberg *et al.* [19] presented a semiempirical formula for the total electron-capture cross section in slow ion-*atom* collisions:

$$\sigma_q^{\rm tot} = C q^\alpha / I_1^\beta. \tag{18}$$

The parameters α, β, and C were found by fitting about 50 absolute experimental cross sections for Xe^{q+}-He, Ar, and Xe collisions yielding the results $\alpha = 0.98 \pm 0.06$, $\beta = 1.96 \pm 0.04$, and $C = (2.7 \pm 0.1) \times 10^{-13}$ cm^2, with I_1 given in eV [19]. This is consistent with the corresponding high-q limit

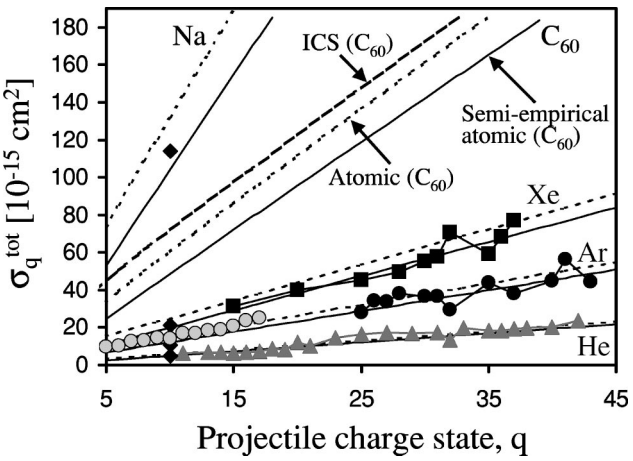

FIG. 8. Absolute and total experimental electron-capture cross sections for Xe^{q+}-He (black triangles), Ar (black circles), and Xe (black squares) from Selberg *et al.* [19]. The gray circles are Ar^{q+}-Ar results of Ali *et al.* [35] and the black diamonds are Xe^{10+}-Na, Xe, Ar and He results of Müller and Salzborn [34]. The solid curves are due to the semi-empirical cross sections [19] for Na ($I_1=5.1$ eV), C_{60} [7.6 eV; Semiempirical atomic (C_{60})], Xe (12.1 eV), Ar (15.8 eV), and He (24.6 eV). The dotted curves are the corresponding atomic over-the-barrier cross sections for Na, C_{60} [Atomic (C_{60})], Xe, Ar, and He [20]. The dashed curve shows the full over-the-barrier ICS results for C_{60}.

values ($\alpha=1$, $\beta=2$, and $C=2.6\cdot 10^{-13}$ cm^2 [19]) derived from the classical over-the-barrier model for atoms using the quasicontinuum assumption [20]. In Ref. [19], the absolute cross section scales were obtained by means of direct measurements of the absolute target pressures using a capacitance manometer (Baratron).

In Fig. 8 we show that the deviations between experimental and the semiempirical results [19] mostly are within $\pm 10\%$ for the atomic targets He [19,34], Ar [19,34,35], Xe [19,34], and Na [34]. This agreement covers a rather wide range of projectile charge states ($5 \leqslant q \leqslant 44$) [5,35], ionization potentials ranging from 5.1 eV (Na) to 24.6 eV (He) [34], and different projectile species [19,35]. The semiempirical results (the solid curves in Fig. 8) lie closely below the over-the-barrier cross sections for atoms [20], represented by the dotted curves. The dashed, dotted, and full curves for C_{60} are the over-the-barrier ICS results over-the-barrier atomic results [20], and the semi-empirical atomic results [19], respectively. In the two latter cases, C_{60} is regarded as an atom, i.e. a pointlike target, with an ionization potential $I_1=7.6$ eV.

We use these three predictions for the total electron-capture cross sections for C_{60} to set upper and lower bounds for the vapor pressure of C_{60}. The model cross sections treating C_{60} as a conducting sphere (πR_1^2; dashed curve) or a pointlike particle ($\pi R_1'^2$; dotted curve) differ little. As pointed out in Sec. III, this shows that polarization and finite-size effects are of some, but still rather limited, importance and that it is a fair approximation to view C_{60} as a pointlike particle for large distance interactions. The semiempirical results lie below, but close to, the over-the-barrier results for the atomic targets. We thus take the semiempirical

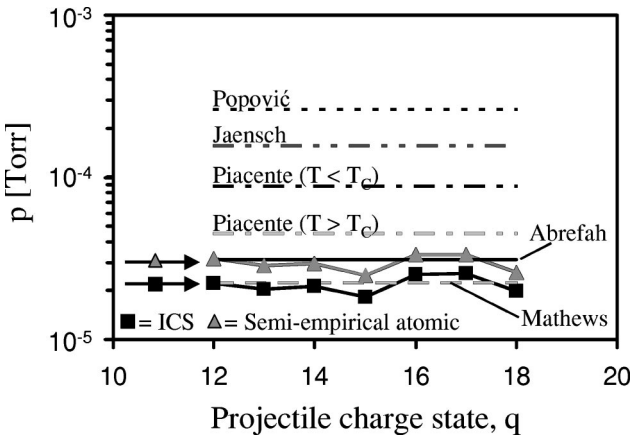

FIG. 9. Upper and lower bounds for the vapor pressure of C_{60} at $T=420\,^\circ$C as functions of q (cf. text). The mean upper and lower bounds are indicated by the arrows to the left. The vapor pressures from Refs. [2,14–17] at $T=420\,^\circ$C are also shown.

results for the hypothetical atomic target with ionization potential $I_1=7.6$ eV to be a lower bound for the true Ar^{q+}-C_{60} cross sections. Similarly, we take the over-the-barrier results using the ICS model for the electronic response of C_{60}, which includes polarization and finite-size effects, as upper bounds for the true cross sections. This is an upper bound since the real finite densities of projectile capture states would tend to make the real cross sections somewhat smaller.

The upper bounds, $\sigma_q^{tot}(\mathrm{ICS})=\pi R_1^2$, give lower limits for the absolute vapor pressure of C_{60} through

$$p_{low}(T)=\frac{k_B T}{\sigma_q^{tot}(\mathrm{ICS})L}\ln(1+S_q). \tag{19}$$

The corresponding upper limits $p_{high}(T)$ are set by the semiempirical (se) cross sections $\sigma_q^{tot}(\mathrm{se})$

$$p_{high}(T)=\frac{k_B T}{\sigma_q^{tot}(\mathrm{se})L}\ln(1+S_q). \tag{20}$$

The individually measured total charge-exchange yields S_q are used to calculate $p_{low}(T)$ and $p_{high}(T)$, which are shown in Fig. 9 for $q=12$–18. The mean values $\langle p_{high}\rangle = 3.0\times 10^{-5}$ Torr and $\langle p_{low}\rangle = 2.2\times 10^{-5}$ Torr are indicated by arrows and compared with the results of Abrefah *et al.* [2], Mathews *et al.* [15], Piacente *et al.* [14], Popovic *et al.* [16], and Jaensch *et al.* [17] at $T=420\,^\circ$C. Note that the vapor pressures by Popovic *et al.* [16] and Jaensch *et al.* [17] are about ten and five times to high, respectively, while those of Abrefah *et al.* [2] and Mathews *et al.* [15] fall close to, or within, the present pressure range.

Larsson *et al.* [5] investigated the temperature dependence of the C_{60} vapor pressure in a collision cell identical to ours (see Fig. 2). When the cell was preheated for several hours at $T_{preh}=500\,^\circ$C, i.e., above the proposed critical temperature $T_C=477\,^\circ$C [13], their charge-exchange yields as functions of temperature were clearly consistent only with the ΔH value of Abrefah *et al.* [2]. This is shown in Fig. 10

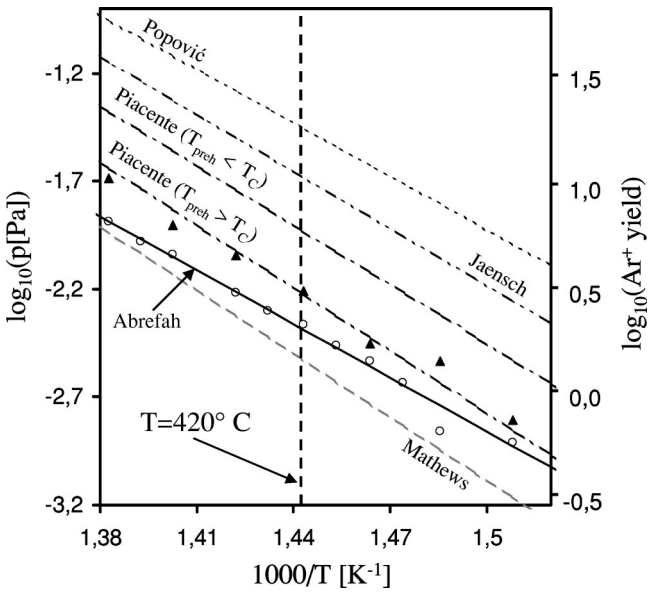

FIG. 10. Vapor pressure relations $\log_{10}(p(T))$ (left scale) as functions of $1/T$ for $T=400-450\,^{\circ}$C: Mathews *et al.* [15] (dashed curve), Abrefah *et al.* [2] (solid curve), Piacente *et al.* [14] with and without preheating above T_C (dash-dotted curves), Jaensch *et al.* [17] (dash-dot-dotted curve), and Popović *et al.* [16] (dotted curve). The right-hand scale shows measurements of the Ar^+ yields due to Ar^{2+}-C_{60} collisions as functions of $1/T$ from Larsson *et al.* [5]. The open circles are the measured Ar^+ yields after heating to 500 °C, and the triangles are similar results without preheating to high temperatures ($T<T_C$).

(the slope is proportional to ΔH), where the left vertical scale gives the logarithm of the vapor pressure and the right vertical scale gives the logarithm of the charge-exchange yields. The open circles are the yields by Larsson *et al.* [5] as a function of $1/T$ for Ar^{2+}-C_{60} collisions after preheating to 500 °C, while the triangles show the corresponding results when the temperature was always kept below 477 °C. The right- and left-hand vertical scales have been shifted to make the open circles fall on the curve by Abrefah *et al.* [2]. Since we use a collision cell and a preheating procedure *identical* to the ones by Larsson *et al.* [5], we base our absolute cross-section scale on Ref. [2] rather than on Ref. [15]. The resulting absolute cross sections are displayed in Fig. 11.

V. DISCUSSION

A. Total-electron-capture cross sections

In Fig. 11 we show the present absolute experimental cross sections together with the model (ICS) and semiempirical results which were used as upper and lower bounds for the absolute cross section scale. We also show the absolute cross sections for Ar^{q+}-C_{60} collisions by Selberg *et al.* [3] for $q=8$, 13, 14, and 15, which were obtained by means of the beam attenuation method [3]. This required rather large variations of the cell temperature and normalization to the incoming beam intensity [3], which yielded larger uncertainties than the present method, described in Sec. II.

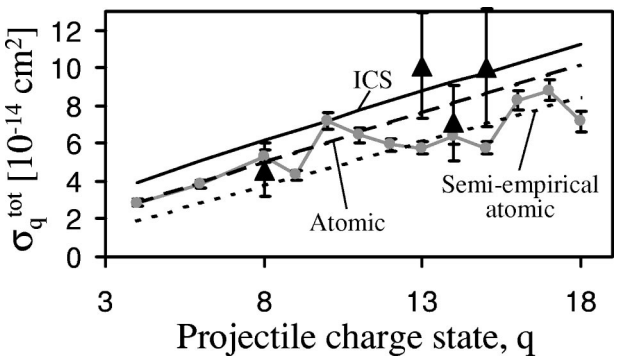

FIG. 11. The present absolute and total electron-capture cross section for Ar^{q+}-C_{60} ($q=4-18$) collisions at $3.3q$ keV (filled circles), based on the vapor pressure [2]. The lines between the data points are to guide the eye. The ICS model cross sections are calculated by the method indicated here and by Cederquist *et al.* [18], and the atomic over-the-barrier results are obtained from Bárány *et al.* [33]. The lower dotted curve is due to the semiempirical formula by Selberg *et al.* [19] assuming that C_{60} is an atom with ionization potential $I_1=7.6$ eV. The triangles are experimental data from Ref. [3].

B. Oscillations in the measured cross sections

The question which now arises from Fig. 11 is if the cross sections falling significantly below the ICS prediction (with the quasicontinuum assumption) can be associated with cases in which the first resonance with a real (Stark shifted) quantum state on the projectile occur well inside the first critical over-the-barrier distance R_1. In order to give a full answer, we would need information about the real densities of states around the values of E_B^1 shown in Fig. 5. This would require a rather extensive set of quantum-mechanical atomic structure calculations, and here we will only deal with the Ar^{18+}-C_{60} case which is particularly simple. The effective principal quantum number for capture of one electron by Ar^{18+} is $n_{eff}^1=14.4$, and the corresponding critical distance is around $R_1=35a_0$, using the ICS model with the quasicontinuum approximation. The outermost real resonance, however, occurs with the purely hydrogenic $n=14$ state in Ar^{17+} at an internuclear distance of about $31a_0$. Within the absorbing sphere picture, we would expect the real absolute cross section to be roughly $(31/35)^2=0.8$ times the ICS value for $q=18$ in Fig. 11. Although crude, this reasoning would account for the low value of this particular cross section. There is no clear correlation between values of n_{eff} far from integer numbers and low experimental cross sections (in relation to the ICS prediction) for $q<18$. This indicates that the true single-electron-capture states are rather far from being hydrogenlike, and that atomic structure calculations are needed in order to resolve this issue. Similar oscillations as functions of q were observed in ion-atom collisions by, e.g., Meyer *et al.* [36].

C. Vapor pressure of C_{60}

The vapor pressure results reported in the literature are all based on one or two of three different methods to measure the rate of C_{60} flow from a temperature controlled cell. These

methods are the following: (i) Measurements of the rate of mass loss from the cell. (ii) Measurements of the torque on a cell emitting C_{60} jets through two orifices on opposite sides of the mounting for a torsion wire. (iii) Direct measurements of the mass flow rate by means of a quartz microbalance some distance from the orifice. Independent of the method used, the measured C_{60} flows must be related to the absolute C_{60} pressures inside the cells. In earlier studies [2,14–16] it was assumed that the flow was also purely effusive at higher temperatures (ranging in some cases up to 600 °C and above). This assumption was criticized by Jaensch *et al.* [17], who stated that the flows could be non-effusive for temperatures well below 500 °C due to very large C_{60}-C_{60} scattering cross sections at thermal velocities [37].

Other main problems, on the side of understanding the flow properties, relate to the evaporation of solvents, the possible restructuring or phase transition in the powder causing a slow decrease of the pressure over longer time periods, and the correct measurement of the equilibrated temperature of the inner wall of the cell [13,17]. In the present study, the temperature was set to a constant value of either 420 or 425 °C for many hours, and we are confident that the equilibrium temperature conditions were fully reached.

In our method to set a range for the C_{60} vapor pressure, we rely partly on the theoretical understanding of single-electron-capture from C_{60} to highly charged ions at large distances. This interaction can be characterized in very simple terms by means of well-established, i.e. experimentally verified, simple classical models. In traditional vapor pressure measurements, however, it appears that a detailed understanding of angular differential scattering in close interactions between excited (hot) neutral C_{60} molecules is needed [17]. This requires extremely advanced fully quantum mechanical calculations [37].

VI. CONCLUSIONS

In this work, we have presented absolute and total experimental electron-capture cross sections for 3.3q-keV Ar^{q+}-C_{60} collisions. The main considerations and conclusions are as follows: (i) The classical over-the-barrier criteron for electron transfer combined with the infinitely conducting sphere model for the electronic response of C_{60}, and an assumption of a quasicontinuum of projectile capture states, are used to define close upper bounds for the total electron-capture cross sections. (ii) Oscillations below this upper bound can most likely be rationalized by lifting the quasicontinuum assumption and to invoke the real quantum structure of the projectile capture states. (iii) Electron capture occurs at large distances and, thus, the total capture cross sections may be approximately described by treating C_{60} as a pointlike object. This approximate treatment gives results only slightly below the ones obtained with the infinitely conducting sphere model. (iv) This leads to the idea that it is possible to use well-established semiempirical cross sections for total electron-capture in ion-atom collisions to estimate the corresponding cross sections for Ar^{q+}-C_{60} collisions. (v) We have set a narrow range for the absolute cross section scale, and thus conclude that the true vapor pressure for C_{60} at 420 °C lies between $\langle p_{low} \rangle = 2.2 \times 10^{-5}$ Torr and $\langle p_{high} \rangle = 3.0 \times 10^{-5}$ Torr. Only the results by Abrefah *et al.* [2] and Mathews *et al.* [15] fall within, or close to these limits and the former has been chosen to set the present absolute cross section scale.

Finally, we note that the most recent C_{60} vapor pressure, by Jaensch *et al.* [17], is much to high—exposing the great difficulties in traditional measurements which rely on modeled relations between the pressure in a cell and the measured C_{60} flow out of that cell. These relations are sensitive to, e.g., poorly characterized thermal C_{60}-C_{60} scattering [17]. Here we have used much simpler, well established, classical pictures for large distance interactions of slow highly charged ions and atoms with C_{60}, and thus reduced the uncertainty in the vapor pressure of C_{60} to 30% at $T = 420$ °C.

ACKNOWLEDGMENTS

The experiment was performed at the Manne Siegbahn Laboratory in Stockholm, and we are grateful to Leif Liljeby and Mikael Björkhage for providing the ion beams. This work was supported by the Swedish Research Council under Contract No. F 650-19981278.

[1] B. Walch, C. L. Cocke, R. Voelpel, and E. Salzborn, Phys. Rev. Lett. **72**, 1439 (1994).
[2] J. Abrefah, D. R. Olander, M. Balooch, and W. J. Siekhaus, Appl. Phys. Lett. **60**, 1313 (1992).
[3] N. Selberg, A. Bárány, C. Biedermann, C. J. Setterlind, H. Cederquist, A. Langereis, M. O. Larsson, A. Wännström, and P. Hvelplund, Phys. Rev. A **53**, 874 (1996).
[4] N. Bohr and J. Lindhard, K. Dan. Vidensk. Selsk. Mat. Fys. Medd. **28**, 7 (1954).
[5] M. O. Larsson, P. Hvelplund, M. C. Larsen, H. Shen, H. Cederquist, and H. T. Schmidt, Int. J. Mass Spectrom. **177**, 51 (1998).
[6] M. S. Baba, T. S. L. Narasimhan, R. Balasubramanian, and C. K. Mathews, Int. J. Mass Spectrom. Ion Processes **114**, R1 (1992).
[7] M. S. Baba, T. S. L. Narasimhan, R. Balasubramanian, and C. K. Mathews, Int. J. Mass Spectrom. Ion Processes **116**, R1 (1992).
[8] A. A. Vostrikov, D. Y. Dubov, and A. A. Agarkov, Pis'ma Zh. Tekh. Fiz. **21**, 73 (1995) [Tech. Phys. Lett. **21**, 715 (1995)].
[9] V. Tarnovsky, P. Kurunczi, S. Matt, T. D. Märk, H. Deutsch, and K. Becker, J. Phys. B **31**, 3043 (1998).
[10] S. Matt, O. Echt, T. Rauth, B. Dünser, M. Lezius, A. Stamatovic, P. Scheier, and T. D. Märk, Z. Phys. D: At., Mol. Clusters **40**, 389 (1997).
[11] Q. Gong, Y. Sun, Z. Huang, X. Zhou, Z. Gu, and D. Qiang, J. Phys. B **29**, 4981 (1996).
[12] A. L. Smith, J. Phys. B **29**, 4975 (1996).
[13] P. F. Coheur, M. Carleer, and R. Colin, J. Phys. B **29**, 4987 (1996).

[14] V. Piacente, G. Gigli, P. Scardala, A. Giustini, and D. Ferro, J. Phys. Chem. **99**, 14 052 (1995).
[15] C. K. Mathews, M. Sai Baba, T. S. Lakshmi Narasimhan, R. Balasubramanian, N. Sivaraman, T. G. Srinivasan, and P.R. Vasudeva Rao, J. Phys. Chem. **96**, 3566 (1992).
[16] A. Popović, G. Dražič, and J. Marsel, Rapid Commun. Mass Spectrom. **8**, 985 (1994).
[17] R. Jaensch and W. Kamke, in Proceedings of the International Workshop on Fullerene and Atomic Clusters, 4–8 October 1999, St. Petersburg, Russia [Mol. Mater. (to be published)].
[18] H. Cederquist *et al.*, Phys. Rev. A **61**, 022712 (2000).
[19] N. Selberg, C. Biedermann, and H. Cederquist, Phys. Rev. A **54**, 4127 (1996).
[20] A. Bárány and C. J. Setterlind, Nucl. Instrum. Methods Phys. Res. B **98**, 184 (1995).
[21] H. Cederquist, A. Fardi, K. Haghighat, A. Langereis, H. T. Schmidt, and S. H. Schwartz (unpublished).
[22] A. Langereis, A. Fardi, K. Haghighat, H. T. Schmidt, S. H. Schwartz, and H. Cederquist (unpublished).
[23] S. Petrie, J. Wang, and D. K. Bohme, Chem. Phys. Lett. **204**, 473 (1993).
[24] H. Shen *et al.*, Phys. Rev. A **52**, 3847 (1995).
[25] D. B. Cameron and J. H. Parks, Chem. Phys. Lett. **272**, 18 (1997).
[26] M. S. Dresselhaus, G. Dresselhaus, and P. C. Eklund, *Science of Fullerenes and Carbon Nanotubes* (Academic Press, San Diego, 1995).
[27] U. Thumm, J. Phys. B **28**, 91 (1995).
[28] U. Thumm *et al.*, Phys. Rev. A **56**, 4799 (1997).
[29] J. U. Andersen and E. Bonderup, Eur. Phys. J. D (to be published).
[30] E. Sohmen, J. Fink, and W. Krätschmer, Z. Phys. B: Condens. Matter **86** 87 1992.
[31] J. U. Andersen *et al.*, Phys. Rev. Lett. **77**, 3991 (1996).
[32] R. Antoine *et al.*, J. Chem. Phys. **110**, 9771 (1999).
[33] A. Bárány *et al.*, Nucl. Instrum. Methods Phys. Res. B **9**, 397 (1985).
[34] A. Müller and E. Salzborn, Phys. Lett. **70A**, 410 (1979).
[35] R. Ali, C. L. Cocke, M. L. A. Raphaelian, and M. Stöckli, Phys. Rev. A **49**, 3586 (1994).
[36] F. W. Meyer, M. Howald, C. C. Havener, and R. A. Phaneuf, Phys. Rev. Lett. **54**, 2663 (1985).
[37] A. Ruiz, J. Breton, and J. M. Gomez Llorente, Chem. Phys. Lett. **270**, 121 (1997).